A General Analytical Method for Calculating Inverter DC-Link Current Harmonics

Brendan Peter McGrath, *Member, IEEE*, and Donald Grahame Holmes, *Senior Member, IEEE*

***Abstract*—Accurate identification of a dc-link ripple current is an important part of switched power-converter design, since the spectral content of this current impacts on dc bus-capacitor lifetime, the stability of the converter control, and the electromagnetic-interference (EMI) performance of the system. Conventionally, the rms magnitude of the ripple current is used to evaluate this impact, but this approach does not readily differentiate between pulsewidth-modulation (PWM) strategies, and can be challenging to evaluate for more complex converter topologies. This paper presents a new generalized approach that analytically determines the harmonic spectrum of the dc-link and dc-bus capacitor currents for any voltage-source switched converter topology. The principle of the strategy is that the product of a phase-leg-switching function and its load current in the time domain, which defines the switched current flowing through the phase leg, can be evaluated in the frequency domain by convolving the spectra of these two time-varying functions. Since PWM has a discrete line-frequency spectrum, this convolution evaluates as an infinite summation in the frequency domain, which reduces to a simple frequency shift of the PWM spectrum when the load current is assumed to be a fundamental single-frequency sinusoid. Hence, the switched currents flowing through the phase legs of an inverter can be evaluated as a summation of harmonics for any PWM strategy or inverter topology and can then be readily combined using superposition to determine the dc-link and dc bus-capacitor currents. The analytical approach has been verified against experimental results for an extensive range of two-level and multilevel converter topologies and PWM strategies.**

***Index Terms*—DC-bus capacitor, dc-link current, double Fourier, multilevel inverter, pulsewidth modulation (PWM), space vector, voltage-source inverter (VSI).**

I. Introduction

THE general structure of a voltage-source inverter (VSI) can be defined as one or more dc voltage sources that connect to the ac output via a network of semiconductor switches. If the duty cycles of the switches are varied using a pulsewidth-modulation (PWM) strategy, the dc source voltage(s) are converted to a train of variable-width pulses with the same volt–second average as the target ac output voltage [1]–[10]. One inevitable consequence of this approach is that the switched output voltage contains a rich spectrum of high-order switching harmonics in addition to the target fundamental component. The analysis of PWM strategies has been the subject of intense research for several decades, and it is now well accepted that the harmonics generated by almost any PWM process can be readily determined using double Fourier series analysis [11].

A second inevitable consequence of using PWM to control an inverter is that the phase-leg switching action causes the (relatively) smooth ac output currents to feed back into the dc link as a train of current pulses [10]. The overall dc bus current is then the superposition summation of the switched current pulses from each phase leg, and, consequently, has a complex harmonic spectrum that is very difficult to accurately analyze [2]–[5]. However, this analysis is important because the dominant factor in the design of the dc bus capacitors is their operational lifetime, which is a function of the surrounding ambient temperature and internal heating caused by the dc-link ripple current flowing through the equivalent series resistance (ESR) of the capacitor [6]. For these reasons, many authors have investigated a variety of analysis techniques to more accurately evaluate the complex dc-link current waveforms of VSIs [2]–[5], [8]–[10].

The presently accepted method for quantifying the dc-link current for a two-level inverter is to calculate the rms magnitude of the dc bus ripple current [3]–[5]. This calculation is based on the duty cycles of the active space vectors and is typically much easier to perform than an exact spectral decomposition of the dc-link current. However, it does not readily discriminate between different PWM strategies [10], even though these strategies are well known to have a strong impact on the harmonic performance of the inverter output and, hence, on the dc-link harmonics [11]. Since the capacitor ESR has a strong frequency dependence [6]–[8], more accurate capacitor loss and lifetime predictions can be made if the dc bus ripple-current spectrum can be accurately calculated for all significant converter operating conditions [6].

This paper presents a general analytical technique for determining the exact harmonic spectrum of the dc-link current of any voltage-fed converter topology under any load condition. The technique recognizes that the spectrum of the switched current flowing through each phase leg is given by the convolution of its corresponding switching-function spectrum with the ac output load-current spectrum. Furthermore, for purely sinusoidal load currents, this spectrum matches that of the corresponding PWM function, frequency shifted by the

Paper 2008-IPPC-100, presented at the 2008 Industry Applications Society Annual Meeting, Edmonton, AB, Canada, October 5–9, and approved for publication in the IEEE Transactions on Industry Applications by the Industrial Power Converter Committee of the IEEE Industry Applications Society. Manuscript submitted for review October 21, 2008 and released for publication February 24, 2009. First published July 17, 2009; current version published September 18, 2009. This work was supported by the Australian Research Council under Project DP0666130 and Project DP0666176.

The authors are with the Electrical and Computer Systems Engineering Department, Monash University, Clayton, Vic. 3800, Australia (e-mail: brendan.mcgrath@eng.monash.edu.au; grahme.holmes@eng.monash.edu.au).

Color versions of one or more of the figures in this paper are available online at http://ieeexplore.ieee.org.

Digital Object Identifier 10.1109/TIA.2009.2027556

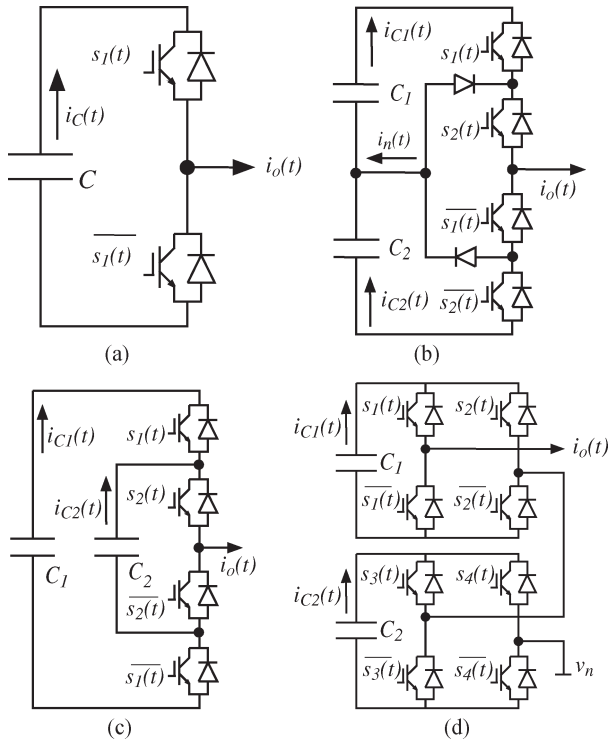

Fig. 1. Voltage-fed converter phase-leg topologies (a) Two-level VSI. (b) Three-level diode-clamped converter. (c) Three-level flying-capacitor converter. (d) Five-level cascaded H-bridge converter.

output fundamental frequency. Using this concept, the well-known spectral performance of two-level [11] and multilevel [12] PWM strategies can be used to calculate the spectrum of the phase-leg switched currents, and the overall dc-link current can then be readily determined using superposition principles.

II. Circuit Analysis of VSIs

The first step in the development of the analytic approach for the quantification of the dc-link current spectrum is to define the instantaneous circuit equations which describe the inverter behavior. To ensure generality, a range of inverter topologies must be considered.

Fig. 1 shows one phase leg for the four common voltage-fed converter topologies of: 1) a two-level VSI; 2) a diode-clamped inverter; 3) a flying-capacitor inverter; and 4) a cascaded H-bridge inverter [1]. If the semiconductor devices are taken to be ideal (i.e., no dead time or saturation voltage drop), the conduction status of any one switch can be represented by the time-varying binary switching function $s(t) \in \{1, 0\}$. Furthermore, the ac output currents can be assumed to be smoothly time varying because of the usual filtering action of the output load impedance.

Under these assumptions, simple circuit analysis identifies the switched currents in the two-level VSI phase leg shown in Fig. 1(a) as

$$i_C(t) = s_1(t) \times i_o(t). \tag{1}$$

Similarly, for the diode-clamped inverter, the switched phase leg currents and the neutral currents of Fig. 1(b) are given by

$$i_{C1}(t) = s_1(t) \times i_o(t) \tag{2}$$

$$i_{C2}(t) = [s_2(t) - 1] \times i_o(t) \tag{3}$$

$$i_n(t) = [s_1(t) - s_2(t)] \times i_o(t). \tag{4}$$

For the flying-capacitor inverter—Fig. 1(c)—the switched phase-leg current and the floating-capacitor current are given by

$$i_{C1}(t) = s_1(t) \times i_o(t) \tag{5}$$

$$i_{C2}(t) = [s_2(t) - s_1(t)] \times i_o(t) \tag{6}$$

and, finally, for the cascaded inverter shown in Fig. 1(d), the intermediate switched phase-leg current equations are given by

$$i_{C1}(t) = [s_1(t) - s_2(t)] \times i_o(t) \tag{7}$$

$$i_{C2}(t) = [s_3(t) - s_4(t)] \times i_o(t). \tag{8}$$

These results show that for all of these converter topologies, the phase-leg switched current waveforms are defined by a simple summation of the products of two time-varying waveforms. Furthermore, when multiple phase legs are combined into a complete inverter system, the overall dc-link current will clearly be just the simple superposition of the time-varying switched current contributions from each phase leg.

Recalling that multiplication in the time domain is equivalent to convolution in the frequency domain, it is clear that if the spectrum of the time-varying signals in (1)–(8) is known, then the spectrum of their time-varying product can be easily determined using a convolution operation in the frequency domain. Now, the frequency spectrum of the switching waveform is defined precisely from PWM theory [11] and needs no further discussion. However, the frequency spectrum of the output load current contains both an output fundamental and harmonic ripple components. If the harmonic ripple components are neglected, the convolution operation is significantly simplified and allows closed-form analytic solutions for the dc-link current to be developed. If the harmonic ripple components are not neglected, closed-form solutions are not possible, but numeric solutions can still be readily evaluated for any particular operating condition.

III. Convolution of the PWM Switching Function and a Sinusoidal Output Current

A considerable body of research now exists concerning the spectral analysis of PWM processes [11]–[14]. It is well accepted that since the PWM process does not generally produce periodic-switching waveforms, a double Fourier series solution is required to analytically quantify the harmonic components of the switched output voltage waveform. The next equation shows the general form of this solution, with a dc component, baseband harmonics (i.e., simple harmonics of the fundamental frequency ω_o), harmonics of the carrier

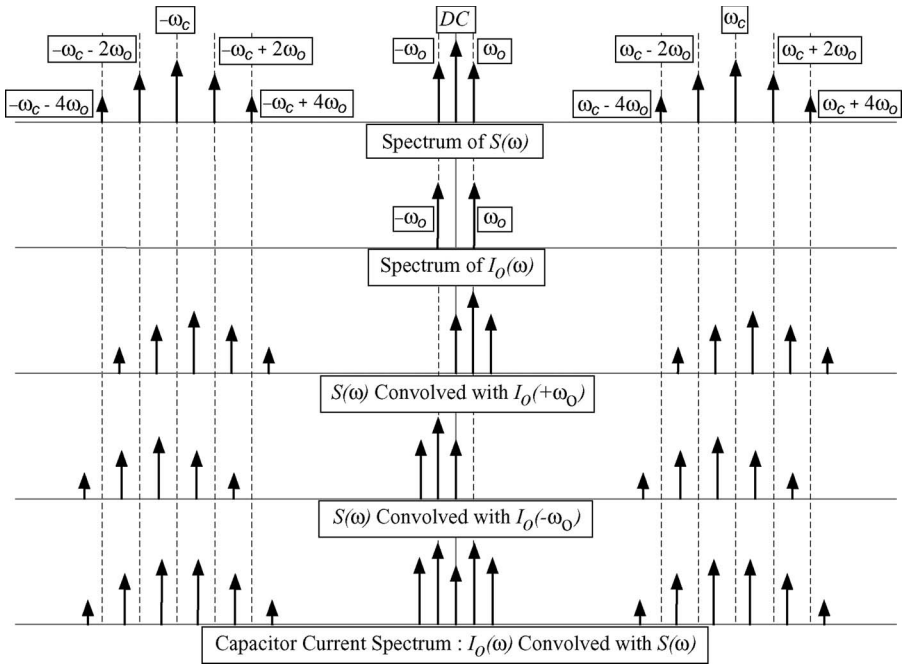

Fig. 2. DC-link current spectrum formed via frequency shifting and summation.

frequency ω_c, and carrier sidebands which cluster around the carrier harmonics [11]

$$s(t) = \frac{A_{00}}{2} + \sum_{n=1}^{\infty} [A_{0n}\cos(n\omega_o t) + B_{0n}\sin(n\omega_o t)] + \sum_{m=1}^{\infty}\sum_{n=-\infty}^{\infty} \big[A_{mn}\cos(m\omega_c t + n\omega_o t) + B_{mn}\sin(m\omega_c t + n\omega_o t)\big]. \quad (9)$$

The spectral coefficients A_{mn} and B_{mn} are defined by a double Fourier integral which must be evaluated for any given modulation strategy and converter topology.

The convolution process can now be illustrated by taking the product term in (1) as an example, which transforms to a convolution integral in the frequency domain of

$$I_C(\omega) = S_1(\omega) \otimes I_o(\omega) = \int_{-\infty}^{+\infty} S_1(\mu) I_o(\omega - \mu)\mathrm{d}\mu. \quad (10)$$

For the case where the load current is a simple sinusoid with a peak value I_o and a power factor ϕ defined by

$$i_o(t) = I_o\cos(\omega_o t + \phi) \quad (11)$$

the integral of (10) becomes

$$I_C(\omega) = \frac{I_o}{2}\left[e^{j\phi}S_1(\omega - \omega_o) + e^{-j\phi}S_1(\omega + \omega_o)\right]. \quad (12)$$

Equation (12) is an important result, since it shows that the spectral content of one phase-leg's contribution to the dc-link current is simply the superposition of the phase-leg's switching-function spectrum with frequency shifts of $\pm\omega_o$. Fig. 2 illustrates this process graphically. The upper trace shows the phase-leg switching-function spectrum up to the first carrier sideband group, while the second trace shows the load-current spectrum. The next two traces show the positively and negatively shifted switching-function spectra, while the lower trace shows the superposition of the frequency-shifted spectra.

Substituting the Fourier transform of (9) into (12) and transforming back to the time domain gives (with some manipulation and consolidation) a Fourier series for the phase-leg switched current of

$$i_C(t) = \frac{\hat{A}_{00}}{2} + \sum_{n=1}^{\infty}\left[\hat{A}_{0n}\cos(n\omega_o t) + \hat{B}_{0n}\sin(n\omega_o t)\right] + \sum_{m=1}^{\infty}\sum_{n=-\infty}^{\infty}\left[\hat{A}_{mn}\cos(m\omega_c t + n\omega_o t) + \hat{B}_{mn}\sin(m\omega_c t + n\omega_o t)\right] \quad (13)$$

where the harmonic coefficients are defined as

$$\hat{A}_{00} = \frac{I_o}{2}[A_{01}\cos\phi + B_{01}\sin\phi] \quad (14)$$

$$\hat{A}_{mn} = \frac{I_o}{2}\big[(A_{m,n-1} + A_{m,n+1})\cos\phi + (B_{m,n-1} - B_{m,n+1})\sin\phi\big] \quad (15)$$

$$\hat{B}_{mn} = \frac{I_o}{2}\big[(B_{m,n-1} + B_{m,n+1})\cos\phi - (A_{m,n-1} - A_{m,n+1})\sin\phi\big]. \quad (16)$$

Equations (13)–(16) are a general analytical result which defines the harmonic components of the switched phase-leg contribution to the dc-link current, based solely on the magnitude

and power factor of the load current and the coefficients of the double Fourier PWM switching function.

To calculate these harmonic components for any other specific converter topology, all that is required is the double Fourier series representation of the converter's PWM strategy and a selection from the product terms (1)–(8) as appropriate for the particular converter topology that is to be considered.

IV. Convolution of the PWM Switching Function With Harmonic Output-Current Components

The analysis in Section III assumed that the harmonic ripple components in the load current were negligible. This assumption considerably simplifies the convolution integral (10) and allows closed-form analytic expressions to be developed for the dc-link current spectrum. Unfortunately, closed-form solutions do not result for cases where the output harmonic ripple current is significant, although the convolution integral in (10) can still be evaluated with useful results. This can be illustrated by considering again a three phase two-level VSI.

For this topology, the switched output phase voltages are

$$v_x(t) = V_{dc} \times s_x(t), \qquad x \in \{a, b, c\}. \tag{17}$$

If a balanced wye-connected load with a phase load impedance of $Z(p)$ is considered (p is the differential operator $p = d/dt$), the inverter output currents are given by

$$Z(p) \begin{bmatrix} i_a(t) \\ i_b(t) \\ i_c(t) \end{bmatrix} = \frac{1}{3} \begin{bmatrix} 2 & -1 & -1 \\ -1 & 2 & -1 \\ -1 & -1 & 2 \end{bmatrix} \begin{bmatrix} v_a(t) \\ v_b(t) \\ v_c(t) \end{bmatrix}. \tag{18}$$

Combining (17) and (18) and taking their Fourier transform gives a complete harmonic definition of the output load current as

$$\begin{bmatrix} I_a(\omega) \\ I_b(\omega) \\ I_c(\omega) \end{bmatrix} = \frac{V_{dc}}{3Z(\omega)} \begin{bmatrix} 2 & -1 & -1 \\ -1 & 2 & -1 \\ -1 & -1 & 2 \end{bmatrix} \begin{bmatrix} S_a(\omega) \\ S_b(\omega) \\ S_c(\omega) \end{bmatrix}. \tag{19}$$

From (19) it can be seen that the output phase current now includes both the target fundamental component and high-frequency ripple components that are related to the switching-function spectrum. Hence, combining (10) and (19) gives a switched phase-leg current spectrum of

$$I_{C\_x}(\omega) = S_x(\omega) \otimes I_x(\omega), \qquad x \in \{a, b, c\}. \tag{20}$$

Since the spectrum of a PWM process is a line spectrum (i.e., an infinite summation of delta functions) rather than a continuous function, the convolution integrals defined by (20) reduce to an infinite summation, which is given by

$$I_{C\_x}(k\omega) = \sum_{h=-\infty}^{\infty} S_x(h\omega) I_x\left([k-h]\omega\right), \qquad x \in \{a, b, c\} \tag{21}$$

for $-\infty < k < +\infty$.

Equation (21) is equivalent to a polynomial multiplication. Hence, it is not practical to use (21) to determine a closed-form analytical solution because of the infinite summation. However, it can be used computationally. Furthermore, many mathematical-analysis packages include functions to perform such a discrete convolution, thereby eliminating the need to explicitly compute the summation of (21).

V. Examples: Analysis of Sine-Triangle PWM

Simple naturally sampled sine-triangle modulation will now be used to illustrate the convolution process for two example converter structures. From [11], the harmonics created by a generalized sine-triangle PWM comparison between a sinusoidal fundamental and a triangular carrier waveform are

$$S_x(t) = \frac{1}{2} + \frac{M}{2}\cos(\omega_o t + \theta_{ox}) + \sum_{m=1}^{\infty}\sum_{n=-\infty}^{\infty}\left[\frac{2}{m\pi}\sin\left([m+n]\frac{\pi}{2}\right) J_n\left(m\frac{\pi}{2}M\right) \times \cos\left(m[\omega_c t + \theta_{cy}] + n[\omega_o t + \theta_{ox}]\right)\right] \tag{22}$$

where $J_n(\xi)$ denotes a Bessel function of the first kind, with order n and argument ξ. The carrier phase angle is θ_{cy}, which is typically set to zero for two-level converters, while the fundamental phase angles are θ_{ox} for $x \in \{a, b, c\}$, with

$$\theta_{oa} = 0 \quad \theta_{ob} = -2\pi/3 \quad \theta_{oc} = +2\pi/3. \tag{23}$$

Sine-triangle PWM, defined in this fashion, is the basis of several multilevel modulation strategies, including, in particular, phase-shifted carrier (PSC) PWM. This strategy is particularly suited to multilevel topologies that are derived from series-connected two-level switching cells (i.e., flying capacitor and cascaded inverters). For an N-level inverter, the PSCPWM method assigns a unique carrier to each of the $N-1$ cells, and a phase shift of $2\pi/(N-1)$ is imposed between each carrier. Intersections between the reference and carrier waveforms define the instantaneous switching states of each cell, and, therefore, the carrier phase angles for each of the $N-1$ switching functions are defined for $y \in \{1, 2, \ldots, (N-1)\}$ as

$$\theta_{cy} = 2\pi(y-1)/(N-1). \tag{24}$$

For the two example converter topologies to be considered, the Fourier coefficients defined by (22) are now substituted into (14)–(16) to obtain the double Fourier series expressions for the dc-link capacitor current as follows:

A. Example No. 1—Two-Level Three-Phase VSI

Since this is a two-level converter, the carrier phase shift θ_{cy} is set to zero. Substituting (22) into (14)–(16) for each phase leg, and, after some consequential algebra, it is found that the switched phase-leg current includes a dc offset, a

fundamental component, a second harmonic, and carrier and sideband harmonics, which for the A-phase are given by

$$\hat{A}_{00} = \frac{M}{4} I_o \cos\phi \quad \hat{A}_{0n} = \hat{B}_{0n} = 0, \qquad n > 2 \tag{25}$$

$$\hat{A}_{01} = \frac{1}{2} I_o \cos\phi \quad \hat{B}_{01} = -\frac{1}{2} I_o \sin\phi \tag{26}$$

$$\hat{A}_{02} = \frac{M}{4} I_o \cos\phi \quad \hat{B}_{02} = -\frac{M}{4} I_o \sin\phi \tag{27}$$

$$\hat{A}_{mn} = \frac{I_o}{m\pi} \cos\left([m+n]\frac{\pi}{2}\right) \cos(\phi) \times \left[J_{n+1}\left(m\frac{\pi}{2}M\right) - J_{n-1}\left(m\frac{\pi}{2}M\right)\right] \tag{28}$$

$$\hat{B}_{mn} = \frac{I_o}{m\pi} \cos\left([m+n]\frac{\pi}{2}\right) \sin(\phi) \times \left[J_{n+1}\left(m\frac{\pi}{2}M\right) + J_{n-1}\left(m\frac{\pi}{2}M\right)\right]. \tag{29}$$

The B- and C-phase contributions to the dc-link current are found by the same way. Summing the contributions from all three phases results in the cancellation of the fundamental, the second harmonic, and all triplen sidebands. Hence, the dc-link current contains only the dc component, carrier harmonics and nontriplen sidebands, with the Fourier coefficients defined by

$$\hat{A}_{00} = \frac{3M}{4} I_o \cos\phi \quad \hat{A}_{0n} = \hat{B}_{0n} = 0, \qquad n \geq 1 \tag{30}$$

$$\hat{A}_{mn} = \frac{I_o}{m\pi} \cos\left([m+n]\frac{\pi}{2}\right) \left[1 + 2\cos\left(n\frac{2\pi}{3}\right)\right] \cos(\phi) \times \left[J_{n+1}\left(m\frac{\pi}{2}M\right) - J_{n-1}\left(m\frac{\pi}{2}M\right)\right] \tag{31}$$

$$\hat{B}_{mn} = \frac{I_o}{m\pi} \cos\left([m+n]\frac{\pi}{2}\right) \left[1 + 2\cos\left(n\frac{2\pi}{3}\right)\right] \sin(\phi) \times \left[J_{n+1}\left(m\frac{\pi}{2}M\right) + J_{n-1}\left(m\frac{\pi}{2}M\right)\right]. \tag{32}$$

B. Example No. 2—Three-Level Flying-Capacitor Converter

The dc-link capacitor current expression for one phase leg of a flying-capacitor converter is defined by (5). When three phases are considered, the dc link and capacitor current will be the summation of the uppermost switch contributions for all three phases. However, since these switching functions have the same carrier phase angle, the capacitor current expression will be the same as for the two-level VSI, and so its spectrum is again defined by (30)–(32).

In contrast, the floating-capacitor current spectrum is quite different, since it is governed by (6). In this case, the switching functions have the same fundamental reference phase angle and a different carrier phase angle. Applying this condition and substituting harmonic terms from (22) into (14)–(16) and then subsequently into (6), it is found that the floating-capacitor current spectrum includes only odd carrier-sideband harmonic terms, which are defined by

$$\hat{A}_{mn} = \frac{I_o}{m\pi} \cos\left([m+n]\frac{\pi}{2}\right) [1 - \cos(m\pi)] \cos(\phi) \times \left[J_{n+1}\left(m\frac{\pi}{2}M\right) - J_{n-1}\left(m\frac{\pi}{2}M\right)\right] \tag{33}$$

$$\hat{B}_{mn} = \frac{I_o}{m\pi} \cos\left([m+n]\frac{\pi}{2}\right) [1 - \cos(m\pi)] \sin(\phi) \times \left[J_{n+1}\left(m\frac{\pi}{2}M\right) + J_{n-1}\left(m\frac{\pi}{2}M\right)\right]. \tag{34}$$

TABLE I
INVERTER CIRCUIT AND MODULATION PARAMETERS

Parameter		Value
DC Link Voltage	(V_{DC})	300 V
Load Inductance	(L_o)	6 mH
Load Resistance	(R_o)	18 Ω
Flying Capacitor (if applicable)	(C_f)	30 μF
Fundamental Frequency	(f_o)	50Hz

VI. THEORETICAL AND EXPERIMENTAL RESULTS

The analytic method previously outlined has been used to calculate the theoretical spectra for the dc-link current for a number of different converter topologies, for a range of PWM strategies. MATLAB was used to perform these calculations, using both closed-form expressions as shown in Section V, and numerical convolution results as described in Section IV. Note that to perform the discrete convolution required in (21), the MATLAB function "`conv`" was used.

To test the validity of the theoretical spectra, experimental tests were done on a two-level VSI and a three-level flying-capacitor inverter. Both inverter systems were controlled using a TMS320C240 DSP, implementing asymmetric regularly sampled PWM. The power stages of both inverter systems were modified to include mechanical standoffs between the bus structure and the dc-link capacitors, allowing the link current to be measured with a current probe. The experimental dc-link current spectra were subsequently obtained using a fast Fourier transform analysis of the measured link current. The inverter parameters and modulation loading conditions for these calculations and experimental tests are given in Table I.

A. Two-Level VSI

The modulation processes for a two-level VSI are well established. Aside from simple sine-triangle modulation, the strategies of particular significance include centered space-vector PWM and discontinuous PWM (DPWM) (i.e., 120°, 60°, and 30°) [11]–[15]. While these techniques are commonly formulated in terms of space-vector theory, they are readily implemented using carrier-comparison techniques, where the phase-leg reference waveforms have a fundamental sine-wave target and a common-mode offset that adjusts the placement of the active space vectors within the switching cycle to achieve the required phase-leg switching states [11]. The reference

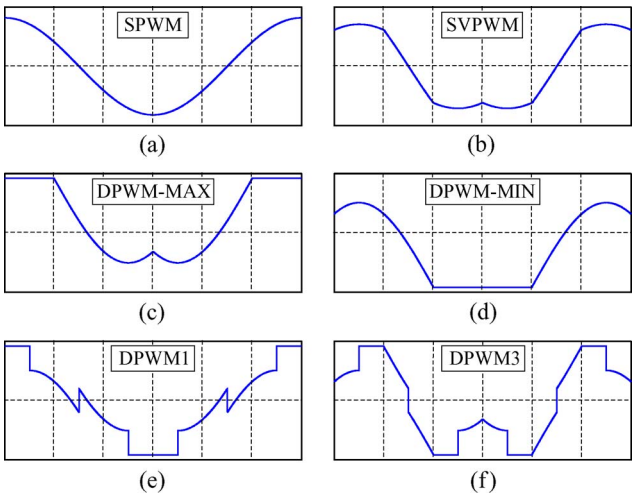

Fig. 3. Phase-A reference waveforms for two-level PWM. (a) sine-triangle PWM. (b) Centered SVPWM. (c), (d) 120° DPWM. (e) 60° DPWM. (f) 30° DPWM.

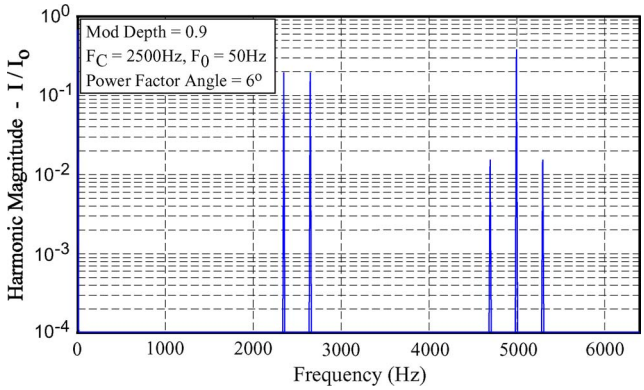

Fig. 4. Two-level VSI (SPWM)—calculated dc-link capacitor-current spectrum via closed-form analytic expressions.

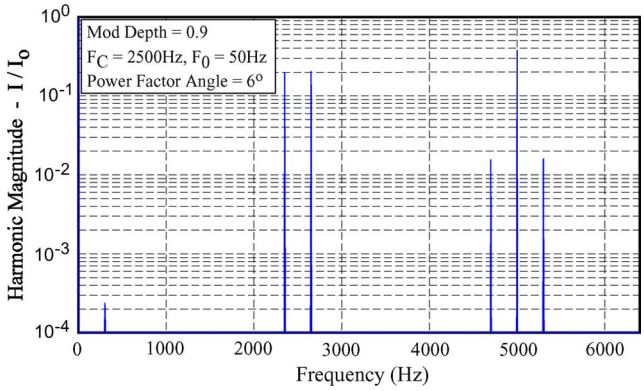

Fig. 5. Two-level VSI (SPWM)—computed dc-link capacitor-current spectrum via the numeric convolution formulas.

waveforms for these PWM strategies are shown in Fig. 3, using the naming conventions of [15].

Figs. 4–6 compare the theoretical and experimental dc-link current spectrum for a sinusoidal PWM (SPWM)-controlled VSI (Note : modulation depth is equivalent to modulation index). The spectrum in Fig. 4 was calculated using the closed-

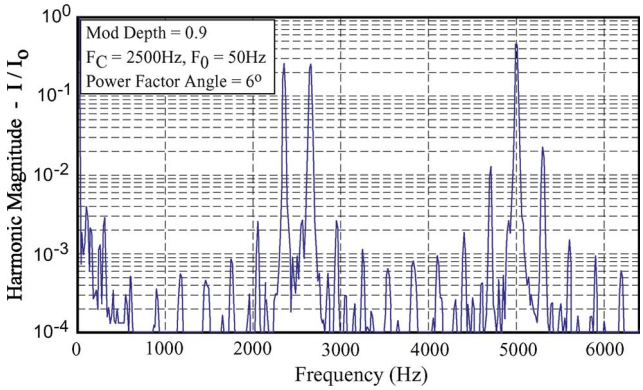

Fig. 6. Two-level VSI (SPWM)—experimental dc-link capacitor current.

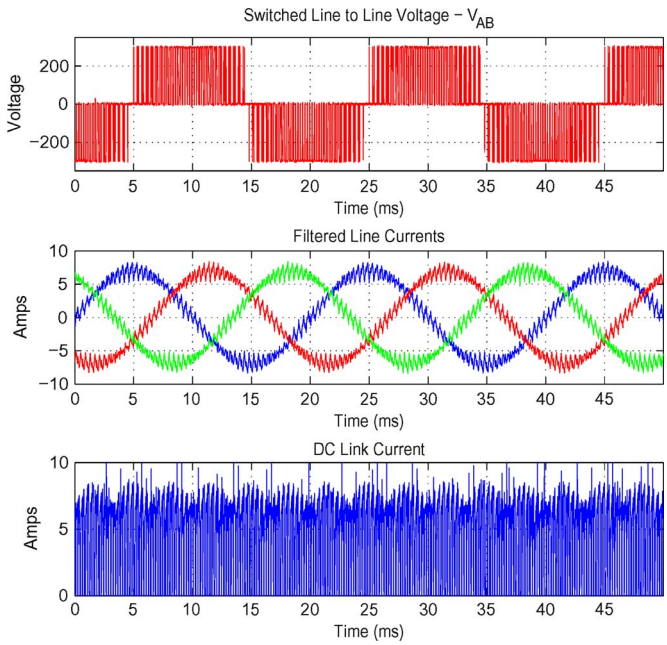

Fig. 7. Two-level VSI (SPWM)—experimental switched waveforms.

form expressions (30)–(32), while the spectrum in Fig. 5 was calculated using the numeric convolution formulas defined by (19) and (21). There is an excellent agreement between the three results, providing a high degree of confidence in the analytic method. Furthermore, the close agreement between Figs. 4 and 5 indicates that there is no significant loss in accuracy by neglecting the ac ripple current for this condition, although the experimental VSI switched waveforms in Fig. 7 show that the ac ripple current can reach as much as 30% of the peak-current value. This suggests that the closed-form dc-link current expressions can be relied upon for most practical inverter systems. Note also that the slight sideband asymmetry observed in the experimental spectrum in Fig. 6 is caused by regular sampling. In principle, the agreement between the analytic and experimental results could be improved by using regular-sampled double Fourier expressions in (30)–(32) [11], but this would be expected to have a minor effect.

The spectral calculation for the space-vector PWM (SVPWM) and DPWM strategies requires the switching-function Fourier series coefficients for each modulation

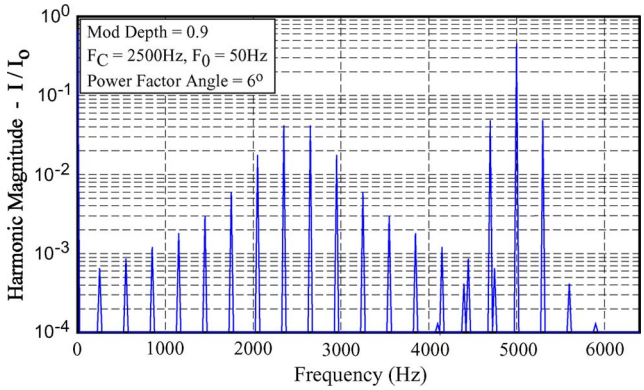

Fig. 8. Two-level VSI (SVPWM)—calculated dc-link capacitor-current spectrum via closed-form analytic expressions.

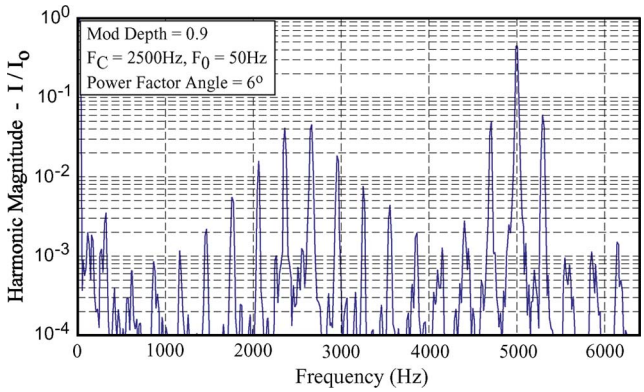

Fig. 9. Two-level VSI (SVPWM)—experimental dc-link capacitor current.

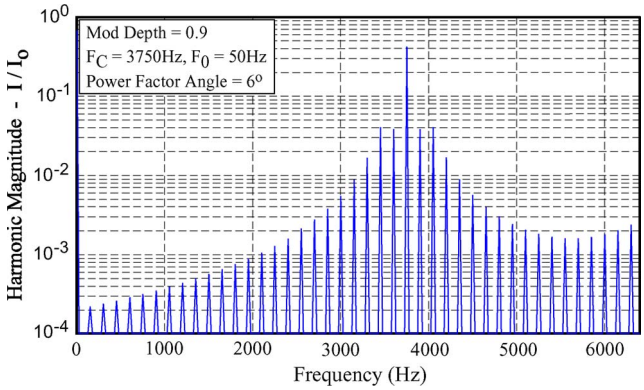

Fig. 10. Two-level VSI (120° DPWM)—calculated dc-link capacitor-current spectrum via closed-form analytic expressions.

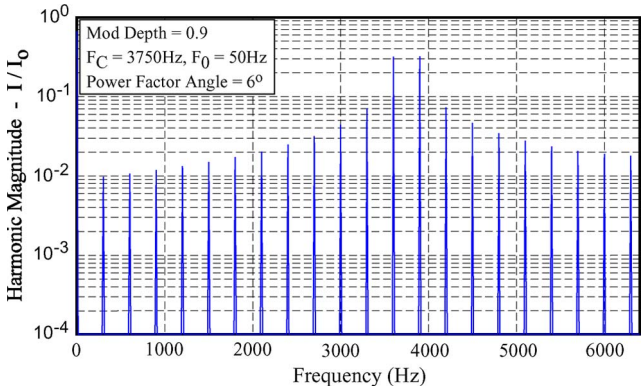

Fig. 11. Two-level VSI (60° DPWM: DPWM1)—calculated dc-link capacitor-current spectrum via closed-form analytic expressions.

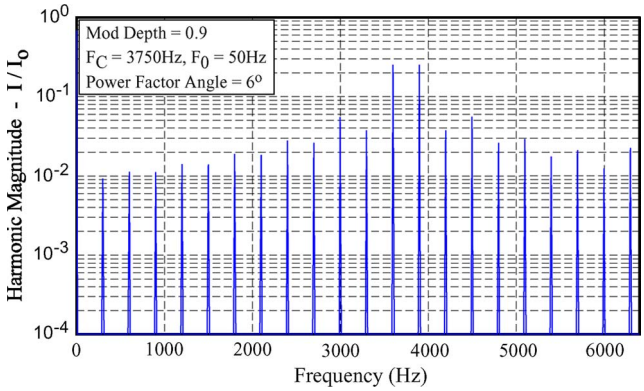

Fig. 12. Two-level VSI (30° DPWM : DPWM3)—Calculated dc-link capacitor-current spectrum via closed-form analytic expressions.

strategy. These coefficients are documented for the SVPWM and 120° discontinuous strategies of [11, p. 282, p. 321]. For the DPWM1 and DPWM3 strategies, the coefficients are readily found using the analysis techniques outlined in [11, Ch. 6]. The coefficients are not presented here due to space limitations.

Figs. 8 and 9 compare the theoretical and experimental dc-link current spectrum for centered SVPWM. The excellent match between these results further validates the analytic approach. Comparing SVPWM with SPWM (Figs. 4–6), it can be seen that the first carrier-sideband group is spread and suppressed in magnitude, while the magnitude of the double carrier-sideband group is increased. This is to be expected, since this is known to occur in the switched output-voltage spectrum for a VSI under SVPWM [11]. It is commented for interest that since the ESR reduces with frequency [6], the shifting of harmonic energy to higher frequency sideband groups may have benefits in terms of the capacitor lifetime.

Figs. 10–12 show the theoretical dc-link current spectra for the DPWM strategies (120° discontinuous, DPWM1, and DPWM3). In all cases, the carrier frequency has been increased by a factor of 3/2 to ensure that the same number of overall switching transitions have been achieved when compared with the continuous PWM methods. In all cases, it is observed that carrier sidebands are now spread considerably. For the DPWM1 and DPWM3 strategies, this spread may well degrade the dc-link capacitor lifetime compared with the continuous PWM methods, since these sidebands intrude into the baseband region at levels of 1% or greater. This is not the case for the 120° discontinuous pattern, although this strategy does introduce a large carrier harmonic at the 40% level which may also have a negative impact on the capacitor lifetime. While exact lifetime calculations are beyond the scope of this paper, the analytic method for calculating the dc-link current spectra offers considerable potential as a design tool when integrated with lifetime-analysis techniques such as the approaches discussed in [6].

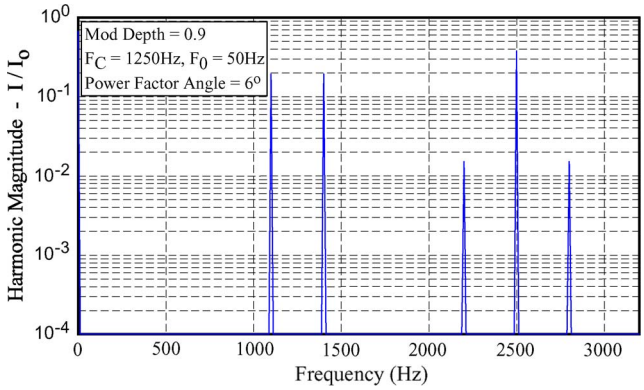

Fig. 13. Three-level flying-capacitor inverter (PSCPWM)—calculated dc-link capacitor-current spectrum via closed-form analytic expressions.

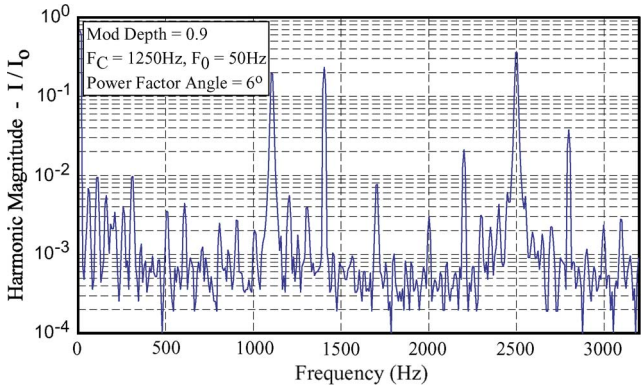

Fig. 14. Three-level flying-capacitor inverter (PSCPWM)—experimental dc-link capacitor-current spectrum.

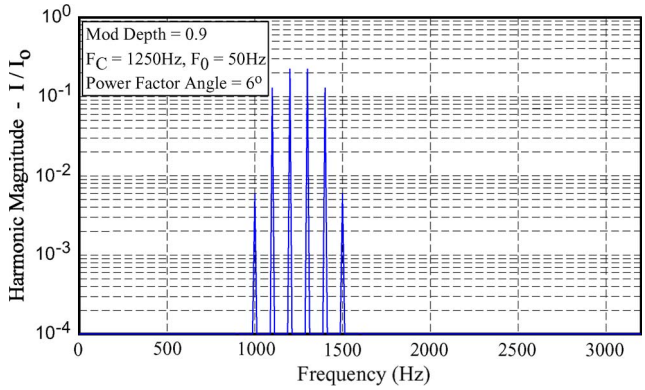

Fig. 15. Three-level flying-capacitor inverter (PSCPWM)—calculated floating-capacitor-current spectrum via closed-form analytic expressions.

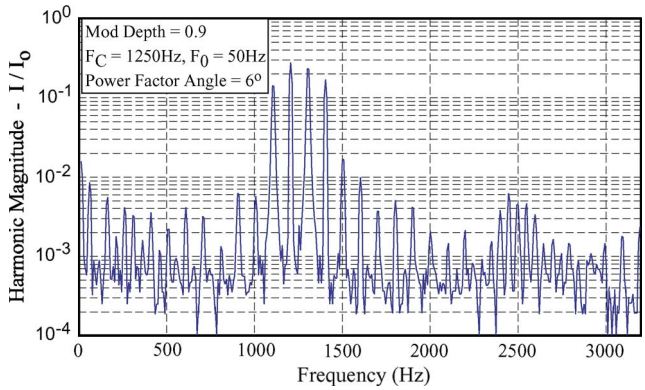

Fig. 16. Three-level flying-capacitor inverter (PSCPWM)—experimental floating-capacitor-current spectrum.

B. Three-Level Flying-Capacitor Inverter—PSCPWM

The dc-link and floating-capacitor current spectra were calculated and measured for a three-phase three-level flying-capacitor inverter employing PSCPWM. Since the PSCPWM strategy increases the effective output ac ripple frequency by a factor of $N-1$, the carrier frequency has been reduced by a factor of two for the three-level system to ensure consistency with the ripple-current conditions for the two-level VSI previously presented. The theoretical spectrum was calculated using the closed-form expressions presented in (30)–(34).

Figs. 13 and 14 compare the theoretical and experimental dc-link current spectra for the flying-capacitor inverter. These spectral results are clearly the same as with the VSI under SPWM (Figs. 4–6), confirming the theoretical prediction presented in Section V. The clear agreement between these results further validates the spectral-analysis technique.

Figs. 15 and 16 compare the analytic and experimental spectra for the floating-capacitor current within one phase leg of the flying-capacitor inverter. There is a clear match between both results, and, as expected, the cancellation of the even carrier-sideband groups and all low-frequency components (i.e., dc, fundamental, etc.) is clearly evident. Note that the imperfect double carrier-sideband-group cancellation observed in the experimental spectrum (Fig. 16) is due to the floating-capacitor ripple voltage, which was observed to reach levels of up to 10% of the dc-link voltage. This imperfect cancellation of sidebands with PSCPWM has previously been described with regard to the switched output-voltage spectrum for cascaded inverters with H-bridge dc-link voltage imbalance [16].

VII. Conclusion

This paper has presented a general analytical technique for determining the spectral components of the dc-link and bus-capacitor currents for dc–ac VSIs. The technique recognizes that the spectral content of the switched current flowing through each phase leg of an inverter is defined by the convolution of the phase-leg's switching-function spectrum and the output load-current spectrum. For sinusoidal load currents, the convolution operation reduces to the superposition of the switching-function spectrum, positively and negatively frequency-shifted by the output fundamental frequency. This allows the well-established double Fourier series results for the modulation of two-level and multilevel inverter topologies to quantify each phase-leg's current pulse-train spectrum. The dc-link current spectrum is then found using superposition principles based on circuit equations for the specific converter topology. When the load current ripple current is significant, the same principle can still be used since PWM switching functions have a line spectrum, which means that the convolution integral reduces to an infinite summation operation. Hence, the convolution operation can be computed numerically by first defining the

inverter load-current equations in terms of the phase-leg switching functions.

The analytic approach has been tested extensively by comparing the analytically calculated spectra against experimental tests performed on a two-level VSI and a three-level flying-capacitor inverter. Modulation strategies including sine-triangle PWM, centered SVPWM, DPWM, and multilevel carrier-based PWM have been investigated, and the analytic results show excellent agreement with the experimental spectra for all cases. It was observed that for loading conditions with a peak-to-peak ripple current up to 30% of the peak ac load current, the closed-form analytic results which neglect the ripple component are sufficiently accurate for the calculation of the dc-link current spectrum.

This spectral-analysis technique is suitable for inverter-design tasks such as the selection of electrolytic capacitors for the inverter dc link based on ripple ratings and lifetime predictions and could also be used to assess dc voltage stability in multilevel inverters (e.g., neutral-point oscillation frequencies in diode-clamped converters).

REFERENCES

[1] J. Rodriguez, S. Bernet, B. Wu, J. O. Pontt, and S. Kouro, "Multilevel voltage-source-converter for industrial medium-voltage drives," *IEEE Trans. Ind. Electron.*, vol. 54, no. 6, pp. 2930–2945, Dec. 2007.

[2] P. Dahono, Y. Sato, and T. Kataoka, "Analysis and minimization of ripple components of input current and voltage of PWM inverters," *IEEE Trans. Ind. Appl.*, vol. 32, no. 4, pp. 945–950, Jul./Aug. 1996.

[3] J. W. Kolar, T. M. Wolbank, and M. Schrödl, "Analytical calculation of the RMS current stress on the DC link capacitor of voltage DC link PWM converter systems," in *Conf. Rec. IEE Int. Elect. Mach. Drives*, 1999, pp. 81–89.

[4] H. Zhang, N. Wheeler, and D. Grant, "Switching harmonics in the DC link current in a PWM AC-DC-AC converter," in *Conf. Rec. IEEE IAS Annu. Meeting*, 1995, pp. 2649–2655.

[5] A. M. Cross, P. D. Evans, and A. J. Forsyth, "DC link current in PWM inverters with unbalanced and non-linear loads," *Proc. Inst. Elect. Eng.—Electr. Power Appl.*, vol. 146, no. 6, pp. 620–626, Nov. 1999.

[6] M. L. Gasperi, "Life prediction modelling of bus capacitors in AC variable-frequency drives," *IEEE Trans. Ind. Appl.*, vol. 41, no. 6, pp. 1430–1435, Nov./Dec. 2005.

[7] F. D. Kieferndorf, M. Forster, and T. A. Lipo, "Reduction of DC-bus capacitor ripple current with PAM/PWM converter," *IEEE Trans. Ind. Appl.*, vol. 40, no. 2, pp. 607–614, Mar./Apr. 2004.

[8] K. Lee, T. Jahns, G. Venkataramanan, and W. Berkopec, "DC-bus electrolytic capacitor stress in adjustable-speed drives under input voltage unbalance and sag conditions," *IEEE Trans. Ind. Appl.*, vol. 43, no. 2, pp. 495–504, Mar./Apr. 2007.

[9] M. N. Anwar and M. Teimor, "An analytical method for selecting DC-link capacitor of a voltage stiff inverter," in *Conf. Rec. IEEE IAS Annu. Meeting*, 2002, pp. 803–810.

[10] M. Bierhoff and F. W. Fuchs, "DC link harmonics of three phase voltage source converters influenced by the pulse width modulation strategy—An analysis," *IEEE Trans. Ind. Electron.*, vol. 55, no. 5, pp. 2085–2092, May 2008.

[11] D. G. Holmes and T. A. Lipo, *Pulse Width Modulation for Power Converters*. Piscataway, NJ: IEEE Press, 2003.

[12] B. P. McGrath and D. G. Holmes, "An analytical technique for the determination of spectral components of multilevel carrier based PWM methods," *IEEE Trans. Ind. Electron.*, vol. 49, no. 4, pp. 847–857, Aug. 2002.

[13] J. F. Moynihan, M. G. Egan, and J. M. D. Murphy, "Theoretical spectra of space-vector modulated waveforms," *Proc. Inst. Elect. Eng.—Electr. Power Appl.*, vol. 145, no. 1, pp. 17–24, Jan. 1998.

[14] D. G. Holmes, "A general analytical method for determining the theoretical harmonic components of carrier based PWM strategies," in *Conf. Rec. IEEE IAS Annu. Meeting*, 1998, pp. 1207–1214.

[15] A. M. Hava, R. J. Kerkman, and T. A. Lipo, "Simple analytical and graphical methods for carrier-based PWM VSI drives," *IEEE Trans. Power Electron.*, vol. 14, no. 1, pp. 49–61, Jan. 1999.

[16] D. G. Holmes and B. P. McGrath, "Opportunities for harmonic cancellation with carrier-based PWM for two-level and multilevel cascaded inverters," *IEEE Trans. Ind. Appl.*, vol. 37, no. 2, pp. 574–582, Mar./Apr. 2001.

Brendan Peter McGrath (M'99) received the B.Sc. degree in applied mathematics and physics, the B.E. degree in electrical and computer systems engineering, and the Ph.D. degree in pulsewidth-modulation theory for multilevel converters from Monash University, Clayton, Australia, in 1997 and 2003, respectively.

After the completion of the Ph.D. degree, he spent two years with Creative Power Technologies, Melbourne, Australia, where he was part of a development team working on auxiliary traction-converter systems and precise utility-instrumentation systems. In 2004, he was a Postdoctoral Researcher with the Laboratoire d'Electrotechnique et d'Electronique Industrielle (LEEI), Toulouse, France, where he worked on the modulation of multicell converters. From 2005 to 2006, he was with the School of Electrical Engineering, University of Newcastle, Newcastle, Australia. Since 2007, he has been with the Department of Electrical and Computer Systems Engineering at Monash University. His principal research interests include the modulation and control of multilevel power converters and the application of signal processing and control theory to power-conversion systems.

Dr. McGrath was the recipient of the Douglas Lampard medal from Monash University for his Ph.D. thesis, in 2004. He is a member of the IEEE Power Electronics, IEEE Industrial Electronics, and IEEE Industry Applications Societies.

Donald Grahame Holmes (M'88–SM'03) received the B.S. and M.S. degrees in power systems engineering from the University of Melbourne, Melbourne, Australia, in 1974 and 1979, respectively, and the Ph.D. degree in pulsewidth-modulation theory for power electronic converters from Monash University, Clayton, Australia, in 1998.

Since 1984, he has been with Monash University, working in the area of power electronics, where he currently heads the Power Electronics Research Group. The present interests of this group include fundamental modulation theory and its application to the operation of energy conversion systems, current regulators for drive systems and PWM rectifiers, active filter systems for quality of supply improvement, resonant converters, current-source inverters for drive systems, and multilevel converters. He has a strong commitment and interest in the control and operation of electrical power converters. He has made a significant contribution to the understanding of PWM theory through his publications and has developed close ties with the international research community in the area. He is the author of over 100 published papers at international conferences and in professional journals and regularly reviews papers for all major IEEE TRANSACTIONS in his area. He has recently coauthored a major reference textbook on PWM theory with Prof. Thomas Lipo of the University of Wisconsin, Madison.

Prof. Holmes is an active member of the Industrial Power Converter Committee and the Industrial Drives Committee of the IEEE Industry Applications Society and a member of the AdCom of the IEEE Power Electronics Society.